Optical Manipulation of a Single Clay Nanosheet Hybridized with a Porphyrin Derivative

YUKI HIGASHI,[1] YASUTAKA SUZUKI,[1,*] TERUYUKI NAKATO,[2] MAKOTO TOMINAGA,[3] JOSEF BREU,[3] TOSHIAKI IWAI,[4] AND JUN KAWAMATA[1]

[1]*Graduate School of Science and Technology for Innovation, Yamaguchi University, 1677-1, Yoshida, Yamaguchi, 753-8512, Japan*
[2]*Department of Applied Chemistry, Kyushu Institute of Technology, 1-1 Sensui-cho, Tobata, Kitakyushu, Fukuoka, 804-8550, Japan*
[3] *Department of Chemistry and Bavarian Polymer Institute, University of Bayreuth, 95447 Bayreuth, Germany*
[4] *Graduate School of Bio-Applications and Systems Engineering, Tokyo University of Agriculture and Technology, 2-24-16 Naka-cho, Koganei, Tokyo 184-8588, Japan*
**ysuzuki@yamaguchi-u.ac.jp*

Abstract: The effect of hybridization of a clay (fluorohectorite (FHT)) nanosheet with a π-conjugated organic compound, α,β,γ,δ-tetrakis(1-methylpyridinium-4-yl)porphyrin p-toluenesulfonate (TMPyP), on its optical manipulation is investigated. Although the hybridized FHT is optically trapped essentially in the same manner as that of neat FHT, the hybridization with TMPyP allows for manipulation of FHT with lower laser intensity or a shorter period, or both. This is ascribed to the larger refractive index and polarizability of TMPyP compared with neat FHT.

1. INTRODUCTION

An optical manipulation technique based on radiation pressure enables noncontact manipulation and nondestructive operation of micro-sized objects, such as glass beads [1], polystylene spheres [2], and bacteria [3]. This technique, therefore, covers many research fields such as materials science [4-6], biological science [7-10], and mechatronics [11-14]. An increase in the radiation pressure results in a stronger ability to grasp an object for optical manipulation.

Nanosheets are regarded as highly anisotropic two-dimensional functional nanomaterials [15-19]. To apply the co-operative effect of their electronic property and structural thinness to electric and opto-electric devices, it is necessary that they can be transported, arranged, and accumulated at will. Our research group has attempted to exploit the optical manipulation behavior of nanosheets. So far, we have revealed that a single nanosheet dispersed in water is optically trapped, whereby the nanosheet is unidirectionally oriented parallel to the propagation direction and the linear polarization plane of the illuminating light [20-23]. Additionally, large structural assemblies of nanosheets can be constructed outside the focal area by means of the inter-particle interactions in liquid crystalline phases that can occur at higher concentrations of the nanosheets [24,25]. We have also attempted to increase the optical radiation pressure by changing the electrical properties of the nanosheets. Based on the research employing nanosheets with different refractive indices, such as fluorohectlite (FHT), niobate nanosheets, and titania nanosheets, it was concluded that the optical radiation pressure exerted on the nanosheet can be increased by increasing the refractive index of the nanosheet. An increase of the optical radiation pressure relating to a higher refractive index contributes to a quicker movement of the nanosheets and lowers the required intensity of the trapping laser beam [21,22].

In this study, we propose an alternative method to increase the radiation pressure applied to a targeted nanosheet by modifying the electronic property of the nanosheets, that is, by hybridization of the nanosheet with a π-conjugated organic compound. Generally, an organic compound equipped with a large π-conjugated system exhibits a stronger interaction with illuminating light compared with inorganic materials, owing to the larger polarizability [26]. Therefore, the response of optical trapping should be enhanced in a hybridized nanosheet compared with that without hybridization. FHT is hybridized with a cationic porphyrin derivative by electrostatic interaction in an aqueous dispersion. A focused laser beam is incident to a colloidal single layer of the hybridized nanosheet. Quick movement of the nanosheet hybridized with the porphyrin is achieved and an optical orientation of the nanosheet parallel to the propagation and polarization direction is observed, similar to the nanosheet without hybridization. Furthermore, the required laser intensity for the optical orientation is significantly lower than that needed in the case of a nanosheet without hybridization. These observations indicate that hybridization with a π-conjugate organic compound increases the optical radiation pressure exerted on the nanosheet. This increase of the optical radiation pressure is ascribed to the larger refractive index and polarizability of TMPyP than those of FHT.

2. EXPERIMENTAL

2.1 Materials

FHT was obtained by melt synthesis followed by long-term annealing, according to an established procedure [27-29]. The nominal composition of the FHT was $[Na_{0.5}]^{inter}[Mg_{2.5}Li_{0.5}]^{oct}[Si_4]^{tet}O_{10}F_2$ and the material featured a cation exchange capacity (CEC) of 1.27 mmol g^{-1}. FHT was dispersed in water to obtain a fully delaminated, all single layer FHT colloid. A porphyrin derivative, α,β,γ,δ-tetrakis(1-methylpyridinium-4-yl)porphyrin *p*-toluenesulfonate (TMPyP; Fig. 1 (left)) was employed as an organic compound because clay-TMPyP hybrid is dispersed in water as a single nanosheet [30-33]. The FHT with TMPyP was prepared by mixing a water dispersion of FHT with an aqueous solution of TMPyP. TMPyP was adsorbed on the FHT surface at a loading of 37% versus CEC. At the loading, the surface coverage of TMPyP on FHT was calculated to be 10% when the TMPyP was assumed to be adsorbed onto the FHT surface without aggregation. FHT hybridized with TMPyP was prepared at a concentration of 0.01 g L^{-1}.

The absorption spectra of colloids of neat FHT and FHT hybridized with TMPyP, obtained by a JASCO V-670-UV-NIR spectrophotometer (JASCO, Tokyo, Japan), using 10-mm quartz cuvettes, are shown in Fig. 1 (right). As for a blank FHT dispersion without TMPyP, a broad spectrum that showed a monotonic increase with the decrease of the wavelength was observed. This arose from light-scattering of the colloidal dispersion. A similar extent of light-scattering of the dispersion of FHT hybridized with TMPyP was also observed in the spectrum. Considering the light-scattering, the light absorption of FHT hybridized with TMPyP at a wavelength region longer than 700 nm was judged as being negligible.

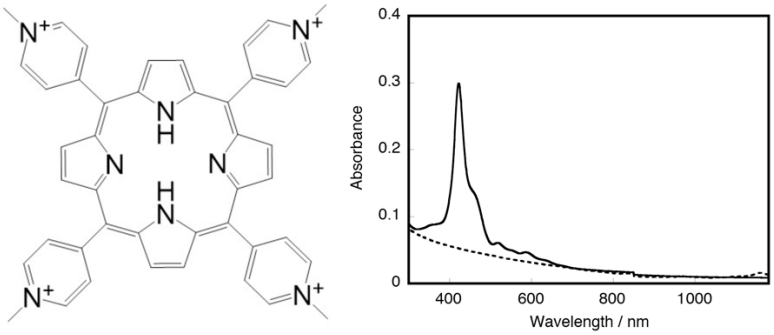

Fig. 1. Chemical structure of TMPyP (left), and absorption spectrum (right) of neat FHT (dashed line) and FHT hybridized with TMPyP (solid line) dispersed in water.

2.2 Optical configuration for optical trapping

Figure 2 shows a schematic representation of the optical configuration. As described, the light absorption of FHT hybridized with TMPyP at the near infra-red region was negligible. To avoid absorption of the laser beam by the hybrid, a linearly polarized continuous-wave (CW) DPSS laser (LSR1064NL, LASEVER, China) oscillating at 1064 nm in the TEM_{00} mode was employed. The colloid samples were injected into a 100-μm-thick thin-layer glass cell. The sample cell was set on the stage of an inverted microscope (IX70, Olympus, Japan). The laser beam was focused on the center of the cell by using an objective lens (Apo, 60×, numerical aperture = 1.20, Olympus). The beam diameter was adjusted to the pupil diameter of the objective lens by using a beam expander. The beam waist size at the focal position was calculated to be 0.33 μm. The sample was simultaneously illuminated by a halogen lamp and the image was monitored by using a digital CMOS camera (ORCA-Flash 4.0 V3, Hamamatsu Photonics, Japan). The incident laser beam was completely blocked by a dichroic mirror and a band pass filter inserted before the camera.

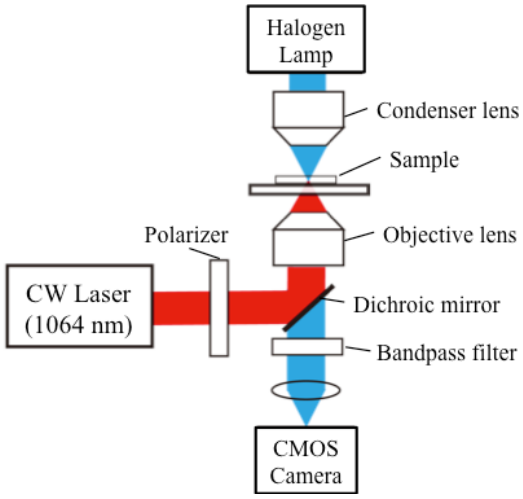

Fig. 2. Schematic representation of the optical configuration.

3. RESULTS AND DISCUSSION

A microscopy observation of the FHTs before and after hybridization of the TMPyP was performed to confirm the hybridization. Figure 3 shows that hybridized FHT was opaque by virtue of the fact that the TMPyP exhibited absorption while neat FHT was transparent. Both the FHT with and without TMPyP were single nanosheets at the present concentration. In addition, TMPyP was assumed to be adsorbed on to FHT homogeneously because FHT with TMPyP (Fig.3(b)) appeared to be uniformly black. These FHT nanosheets moved three-dimensionally with Brownian motion. Thus, the FHT nanosheets were sometimes clearly observed but sometimes were blurred because their motion moved them in and out of focus. Brownian motion was essentially the same as for neat FHT (see Visualizations 1 (neat FHT) and 2 (hybridized FHT)).

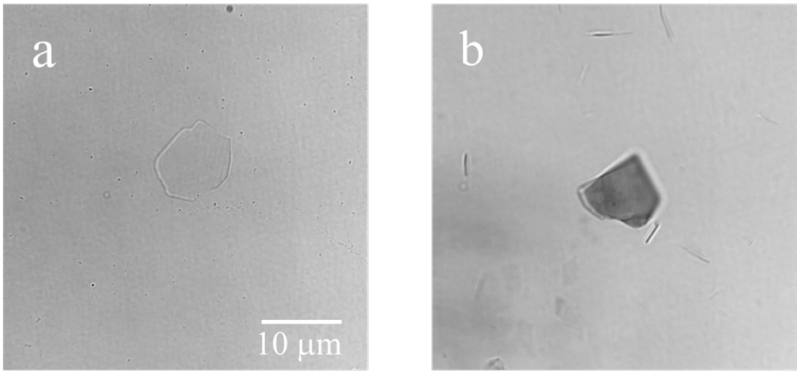

Fig. 3. Microscopy images of (a) neat FHT and (b) FHT hybridized with TMPyP.

The effect of hybridization on the dynamics of optical manipulation behavior was investigated through optical microscopy observations. The optical microscopy images of neat FHT and FHT with TMPyP before and after illumination by a linearly polarized laser beam are shown in Fig. 4, Visualizations 3 (neat FHT) and 4 (hybridized FHT). As described later, the required laser power for manipulating a nanosheet depends on the size of nanosheet. Thus, the sizes of neat FHT and FHT with TMPyP exemplified in Fig. 4 were almost identical with areas of 92 and 89 μm^2, respectively. Figure 4a and 4f shows the microscopy images of neat FHT and FHT with TMPyP before laser illumination. The nanosheets oriented with their in-plane direction parallel to the focal plane. Upon continuous illumination of a 15-mW laser beam, the FHT and FHT with TMPyP started tilting toward the direction perpendicular to the focal plane; that is, parallel to the propagation direction of the laser beam (Fig. 4d, 4g). The final orientation of the nanosheet edge was parallel to the polarization direction of the incident laser beam (Fig. 4e, 4h–4j). The behavior of the FHT with TMPyP under laser illumination was essentially the same as for other nanosheet materials [21]. However, FHT with TMPyP could be manipulated more quickly than neat FHT. FHT with TMPyP started tilting only 7 s after switching on the continuous laser illumination (Fig. 4g). The orientation of FHT with TMPyP was completed within as little as 10 s (Fig. 4h). However, in the case of FHT without TMPyP, 230 s of beam illumination was required for tilting (Fig. 4d) and orientation was completed after 240 s (Fig. 4e). Thus, the hybridization of FHT with TMPyP drastically decreased the required time for completing the optical manipulation of FHT.

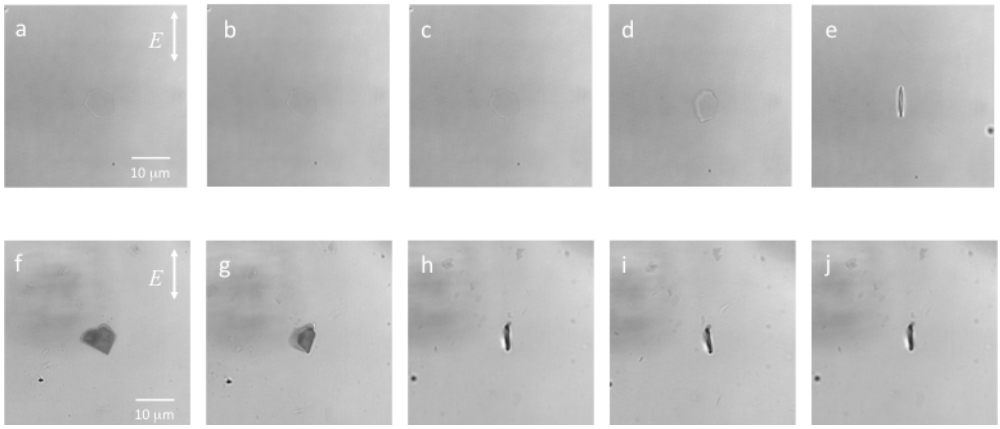

Fig. 4. Bright-field optical microscopy images of (a–e) neat FHT and (f–j) FHT with TMPyP when illuminated by a 15 mW laser beam. These images indicate (a, f) before illumination and after (b, g) 7 s, (c, h) 10 s, (d, i) 230 s and (e, j) 240 s of continuous laser illumination. The white double arrows indicate the polarization direction.

Although the thickness of FHT was only 0.95 nm, the edge of FHT is clearly observed in Fig. 4. The most probable reason for the observation of such a small sized edge was the considerably larger lateral size (5–20 μm) of the trapped FHT compared with the focal depth (0.3 μm) of the objective lens. Because the focal depth was significantly smaller than the lateral size of FHT, both edges of the FHT were located far from the focal depth of the objective lens when the FHT was oriented with its in-plane direction parallel to the propagation direction of the laser beam and the focal depth was set to the center of FHT. Thus, the image of the edges should be blurred. Owing to this defocusing of the edges, the single FHT was observed as if it was a thin object.

Repeatability of the optical manipulation behavior was confirmed through on-off switching of the laser beam. Figure 5 exemplifies the microscopy observations of the optical trapping behavior of hybridized FHT by repeated on-off switching of the laser beam. The trapped FHT with TMPyP was gradually relaxed by Brownian motion when the laser illumination was ceased. The nanosheet trapped at the focal point began to be positionally and orientationally shifted just after stopping the laser illumination. The nanosheet was then gradually moved and tilted in the direction parallel to the focal plane. As shown in Fig. 5 (c), a similar orientation of the nanosheet to that before commencing laser illumination was observed 300 s after stopping the laser illumination. The FHT with TMPyP was repeatedly trapped at the focal point by on-off switching of the laser illumination. As shown in Fig. 5 (d), the appearance of hybridized FHT after 20 cycles of on-off switching of the laser beam was almost unchanged compared with that before laser illumination. This observation indicated that decomposition of TMPyP arising from the laser illumination had not occurred for at least 20 cycles of on-off switching of the laser illumination.

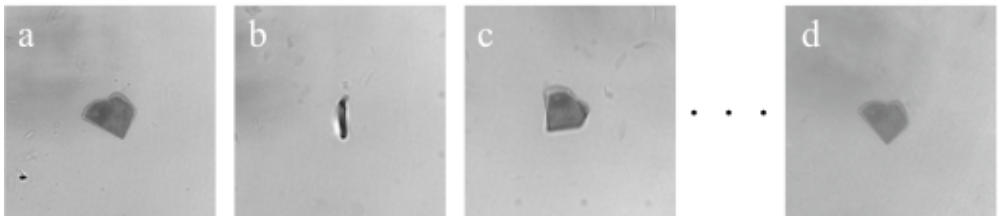

Fig. 5. Optical microscopy images of the repeatedly trapped FHT hybridized with TMPyP by on-off switching of the laser illumination. Before laser irradiation (a), after 300 s of continuous laser illumination (b), 300 s after laser illumination was ceased (c) and after 20 cycles of on-off switching of the laser illumination (d).

To discuss the dependence of the nanosheets in laser manipulation on the illuminating laser power, Fig. 6 schematically shows the dynamics of the nanosheet under illumination of a focused laser beam. Figure 6(a) corresponds to (a)–(c) and (f) in Fig. 4, Fig. 6(b) to (d) and (g) in Fig. 4, and Fig. 6(c) to (e) and (h)–(j) in Fig. 4. The resultant radiation force of the scattering and the gradient forces were related to the optical manipulation of the nanosheet. The former primarily worked in the transition process from the initial condition shown in Fig. 6(a) to the rotation shown in Fig. 6(b); the latter worked more dominantly with an increase in the area of the nanosheet inside the electric field of the illuminating beam shown from Fig. 6(b) to Fig. 6(c).

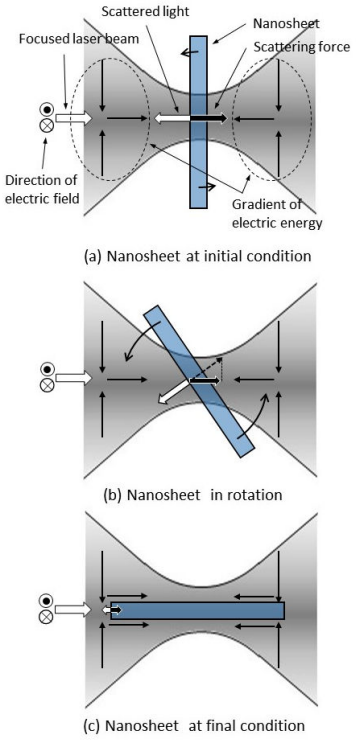

Fig. 6. Schematic diagram of nanosheet dynamics under illumination of a focused laser beam.

The radiation force induced by light scattering is given by [34]

$$F = Q_{pr}\frac{n_1 P}{c} \tag{1}$$

where n_1P/c is the incident momentum per second of a ray of power P in a surrounding medium with a refractive index of n_1, and c is the speed of light in a vacuum. The quantity Q_{pr} is the efficiency factor for radiation pressure that is the dimensionless constant given by the cross-section C_{pr} of the scatterer for radiation pressure divided by the geometrical cross-section. The radiation pressure cross-section is given by

$$C_{pr} = C_{ext} - gC_{sca} = (1-g)C_{sca} + C_{abs} \tag{2}$$

where C_{ext}, C_{sca} and C_{abs} are the cross sections of the scatterer for extinction, scattering, and absorption, respectively. g is the mean cosine of the scattering angle θ weighted with the scattering phase function $p(\theta)$ and defined by

$$g = 2\pi \int_0^{\pi} \cos\theta p(\theta) \sin\theta d\theta. \quad (3)$$

As shown in Fig. 1, the absorption cross-section is negligible at the wavelength 1064 nm of the laser source used in the manipulation and the radiation pressure cross-section is approximately given by

$$C_{pr} = (1 - g)C_{sca}. \quad (4)$$

The dependence of the minimum laser power on the size and refractive index of the scatterer may arise from the fact that the forward momentum of the scattered light is proportional to the magnitude of the isotropic component in scattering, as shown in Eq.(2). Table 1 shows the minimum laser power required to manipulate neat and hybridized FHT within 300 s. We tested 5 samples in each of the particle-size ranges. All tested nanosheets could be manipulated essentially in the same manner as shown in Fig. 4. Owing to a large variation of particle shape, it was found that the minimum laser powers required for manipulations of both the neat FHT and hybridized FHT did not consistently increase with their size. Referring to the numerical calculation based on the Mie theory, the radiation pressure for a nano-sized object increases consistently with the illuminating laser power [35] but does not increases in the same manner for micro-sized object [36]. In fact, the sizes of the nanosheets (in-plane direction) were in the Mie theory region and the sizes were much larger than the spot size of the illuminated laser beam. This meant the absolute value of radiation pressure applied to the nanosheet was constant even though the size of the nanosheet varied. Thus the factor that determined the size dependence in Table 1 was proposed to be the viscous resistance of a solvent. This is because the viscous resistance that operates on nanosheets during transitional and rotational movement of the nanosheet should be increased with the increase in the size of the nanosheets. The minimum laser power required for optical manipulation was clearly smaller for the hybridized FHT than the neat FHT. This was considered to be related to the effect of hybridization because both the neat and hybridized FHT were transparent (i.e., nonabsorbent) at the wavelength of 1064 nm. The scattering cross-section and *g*-parameter in Eq. (4) depends only on the refractive index of the scatter because the illuminating beam size was much smaller than the size of the nanosheets from the initial condition shown in Fig. 6(a) to the middle of the rotation shown in Fig. 6(b). The typical refractive index of clay minerals is 1.5, as has been reported in the previous works [37, 38], and the mutual refractive index of FHT suspended in water is 1.1. In contrast, π-conjugated molecules generally have a higher refractive index than that of clay minerals. In fact, TMPyP has been reported to have a refractive index of 1.7 [39] and, consequently, the mutual refractive index of TMPyP is 1.3. The difference in the mutual refractive index should be a reason why FHT with TMPyP can be manipulated more quickly even by low power laser beam illumination compared with neat FHT.

Table 1. Minimum laser power required to manipulate neat FHT and FHT with TMPyP within 300 s.

Particle Size / μm^2	Minimum Laser Power / mW	
	FHT	FHT with TMPyP
50 ~ 100	12 ~18	5 ~ 8
100 ~ 150	17 ~ 22	7~ 10
150 ~ 200	18 ~ 23	8 ~ 12

We next considered the relationship of another force—the gradient force—with the polarizability of the scatter. The gradient force is written as the following expression [40-43];

$$U = \frac{1}{2}\alpha \nabla E^2 + \frac{\partial}{\partial t}(\boldsymbol{E} \times \boldsymbol{B}) \qquad (5)$$

where $\boldsymbol{E}$ and $\boldsymbol{B}$ are the electric field density and the magnetic flux density of the illuminating laser beam, respectively, and α is the polarizability of the scatter. The second term is practically zero on average when the light field is detected for a finite response time. Because porphyrin derivatives are equipped with large π-conjugation systems, their π-electrons can be significantly delocalized when an alternative electric field of a laser beam is applied. This characteristic results in the large polarizabilities (α) of porphyrin derivatives [44]. Thus, the polarizability of FHT with TMPyP should be higher than that of neat FHT. Therefore, the first term in Eq. (5) can become extremely large because the gradient of the electric field can be enhanced in the beam waste area that is created by a high-NA objective lens.

The dependency of the temporal response in optical manipulation on the laser intensity is considered to be related directly with the gradient force. The relationship between the required times for optical trapping and the laser intensity is summarized in Table 2. When illuminating the same samples shown in Fig. 4a and 4f with a laser beam intensity of 8 mW, 150 s were required for complete orientation of FHT with TMPyP, whereas neat FHT could not be trapped at all even with continuous irradiation for more than 600 s. When the power of the laser beam was lowered further to 5 mW, then neither neat FHT nor FHT with TMPyP could be trapped even with 600 s of continuous laser illumination. The gradient force makes it possible to manipulate the FHT with TMPyP more quickly under a low-power illumination compared with neat FHT. In addition, the gradient force will act on the stable rotation of the nanosheet because it acts on an extremely narrow area of the nanosheet around the focal point from opposite directions, as shown in Fig. 6.

Table 2. Laser power and time required for the optical trapping of 92 μm^2 of neat FHT and 89 μm^2 of FHT with TMPyP.

	Laser Power / mW	Time / s
FHT	8	∞
	15	240
FHT with TMPyP	8	150
	15	10

4. CONCLUSIONS

This study provides a novel technique for the quick and low power on-demand orientation manipulation of nanosheets. By hybridizing with an organic compound of high refractive index and large polarizability, the nanosheet can be manipulated quickly even with a low power laser beam. By applying this methodology to the large variety of combinations of nanosheet materials and organic compounds, much easier orientation manipulation of nanosheets should be realized.

Furthermore, we have demonstrated optical manipulation of a clay nanosheet hybridized with an organic compound. To fully explore the functionality of hybrids, the development of a methodology that enables local and on-demand orientation manipulation of hybrids is strongly required. Manipulation of hybrids, as established in this study, should be a powerful tool to realize local and on-demand orientation manipulation of hybrids.

Unfortunately, a quantitative discussion on the polarizability of the nanosheet cannot be made from the work despite the importance of this parameter. Generally speaking, a polarizability measurement of the nanosheet is quite difficult owing to the chemical and physicochemical complexities of the nanosheet and its aqueous suspension. We would expect

a possibility that the polarizability of the nanosheet can be measured by estimating the temporal dynamics of the optical manipulation through this research.

Funding

This work was supported by JSPS KAKENHI (No. 19H02689, 19K05403, 19H04677).

Acknowledgements

The authors gratefully acknowledge Ms. Misato Suehisa and Mr. Hiroaki Yahara (Yamaguchi University) for their support with the experiments. We thank Edanz Group (www.edanzediting.com/ac) for editing a draft of this manuscript.

Disclosures

The authors declare no conflicts of interest.

References

1. A. Ashkin, J. M. Dziedzic, J. F. Bjorkholm and S. Chu, "Observation of a single-beam gradient force optical trap for dielectric particles," Opt. Lett. **11**(5), 288–290 (1986).
2. J. Won, T. Inaba, H. Masuhara, H. Fujiwara, K. Sasaki, S. Miyawaki and S. Sato, "Photothermal fixation of laser-trapped polymer microparticles on polymer substrates," Appl. Phys. Lett. **75**(11), 1506–1508 (1999).
3. A. Ashkin and J. M. Dziedzic, "Optical trapping and manipulation of viruses and bacteria," Science **235**(4795), 1517–1520 (1987).
4. S. M. Block, L. S. B. Goldstein and B. J. Schnapp, "Bead movement by single kinesin molecules studied with optical tweezers," Nature **348**, 348–352 (1990).
5. H. Misawa, M. Koshioka, K. Sasaki, N. Kitamura and H. Masuhara, "Three-dimensional optical trapping and laser ablation of a single polymer latex particle in water," J. Appl. Phys. **70**(7), 3829–3836 (1991).
6. K. Svoboda and S. M. Block, "Optical trapping of metallic Rayleigh particles," Opt. Lett. **19**(13), 930–932 (1994).
7. J. T. Finer, R. M. Simmons and J. A. Spudich, "Single myosin molecule mechanics: piconewton forces and nanometre steps," **368**, Nature 113–119 (1994).
8. H. Li, D. Zhou, H. Browne and D. Klenerman, "Evidence for resonance optical trapping of individual fluorophore-labeled antibodies using single molecule fluorescence spectroscopy," J. Am. Chem. Soc. **128**(17), 5711–5717 (2006).
9. Y. Tsuboi, T. Shoji and N. Kitamura, "Optical trapping of amino acids in aqueous solutions," J. Phys. Chem. C **114**(12), 5589–5593 (2010).
10. T. Shoji, N. Kitamura and Y. Tsuboi, "Reversible photoinduced formation and manipulation of a two-dimensional closely packed assembly of polystyrene nanospheres on a metallic nanostructure," J. Phys. Chem. C **117**(6), 10691–10697 (2013).
11. M. D. King, K. C. Thompson and A. D. Ward, "Laser tweezers raman study of optically trapped aerosol droplets of seawater and oleic acid reacting with ozone: implications for cloud-droplet properties," J. Am. Chem. Soc. **126**(51), 16710–16711 (2004).
12. N. Murazawa, S. Juodkazis, S. Matsuo and H. Misawa, "Control of the molecular alignment inside liquid crystal droplets by use of laser tweezers," Small **1**(6), 656–661 (2005).
13. K. Inaba, K. Imaizumi, K. Katayama, M. Ichiyama, A. Ashida, T. Iida, H. Ishihara and T. Itoh, "Optical manipulation of CuCl nanoparticles under an excitonic resonance condition in superfluid helium," Phys. Stat. Sol. **243**(14), 3829–3833 (2006).
14. A. Ohlinger, S. Nedev, A. A. Lutich and J. Feldmann, "Optothermal escape of plasmonically coupled silver nanoparticles from a three-dimensional optical trap," Nano Lett. **11**(4), 1770–1774 (2011).
15. H. Ajiki, T. Iida, T. Ishikawa, S. Uryu and H. Ishihara, "Size- and orientation-selective optical manipulation of single-walled carbon nanotubes: a theoretical study," Phys. Rev. **80**, 115437 (2009).
16. N. Miyamoto and T. Nakato, "Liquid crystalline nanosheet colloids with controlled particle size obtained by exfoliating single crystal of layered niobate $K_4Nb_6O_{17}$," J. Phys. Chem. B **108**(20), 6152–6159 (2004).
17. T. Nakato, K. Nakamura, Y. Shimada, Y. Shido, T. Houryu, Y. Iimura and H. Miyata, "Electrooptic eesponse of colloidal liquid crystals of inorganic oxide nanosheets prepared by exfoliation of a layered niobate," J. Phys. Chem. C **115**(18), 8934–8939 (2011).
18. T. Nakato, Y. Nono, E. Mouri and M. Nakata, "Panoscopic organization of anisotropic colloidal structures from photofunctional inorganic nanosheet liquid crystals," Phys. Chem. Chem. Phys. **16**, 955–962 (2014).
19. T. Nakato, Y. Nono and E. Mouri, "Textural diversity of hierarchical macroscopic structures of colloidal liquid crystalline nanosheets organized under electric fields," Colloid Surf. A **522**(5), 373–381 (2017).

20. M. Tominaga, Y. Higashi, T. Kumamoto, T. Nagashita, T. Nakato, Y. Suzuki and J. Kawamata, “Optical trapping and orientation manipulation of 2D inorganic materials using a linearly polarized laser beam,” Clays and Clay Minerals **66**, 138–145 (2018).
21. Y. Higashi, T. Nagashita, T. Nakato, Y. Suzuki and J. Kawamata, “A Laser beam induced optical manipulatin of a smectite,” Clay Sci. **22**(3), 79–83 **(**2018).
22. T. Nakato, K. Saito, A. Ikeda, Y. Higashi, Y. Suzuki and J. Kawamata, “Optical trapping of inorganic oxide nanosheets colloidally dispersed in water: effects of refractivity,” Clay Sci. **23**(2), 25–30 (2019).
23. T. Nakato, Y. Higashi W. Ishitobi, T. Nagashita, M. Tominaga, Y. Suzuki, T. Iwai, J. Kawamata, “Microscope observation of morphology of colloidally dispersed niobate nanosheets combined with optical trapping,” Langmuir **35**(16), 5568–5573 (2019).
24. M. Tominaga, T. Nagashita, T. Kumamoto, Y. Higashi, T. Iwai, T. Nakato, Y. Suzuki and J. Kawamata, “Radiation pressure induced hierarchical structure of liquid crystalline inorganic nanosheets” ACS Photonics **5**(4), 1288–1293 (2018).
25. T. Nagashita, Y. Higashi, A. Ikeda, M. Tominaga, T. Kumamoto, Y. Suzuki, T. Nakato and J. Kawamata, “Laser beam induced orientation control of a nanosheet liquid crystal by employing an objective lens with a low numerical aperture,” Clay Sci. **22**(1), 13–17 (2018).
26. D. S. Chemla and J. Zyss, *Nonlinear Optical Properties of Organic Molecules and Crystals Volume 2* (Academic Press, Orlando, 1987), Chap. III-5.
27. M. Stöter, D. A. Kunz, M. Schmidt, D. Hirsemann, H. Kalo, B. Putz, J. Senker and J. Breu, “Nanoplatelets of sodium hectorite showing aspect ratios of approximately 20,000 and superior purity,” Langmuir **29**, 1280–1285 (2013).
28. S. Rosenfeldt, M. Stöter, M. Schlenk, T. Martin, R. Q. Albuquerque, S. Förster and J. Breu, “In-depth insights into the key steps of delamination of charged 2D nanomaterials,” Langmuir **32**, 10582–10588 (2016).
29. J. Breu, W. Seidl, A. J. Stoll, K.G. Lange and T. U. Probst, “Charge homogeneity in synthetic fluorohectorite,” Chem. Mater. **13**(11), 4213–4220 (2001).
30. Z. Chernia and D. Gill, “Flattening of TMPyP adsorbed on laponite. evidence in observed and calculated UV−vis spectra,” Langmuir **15**(5), 1625–1633 (1999).
31. P. M. Dias, D. L. A. De Faria and V. R. L. Constantino, “Spectroscopic studies on the interaction of tetramethylpyridylporphyrins and cationic clays,” J. Incl. Phenom. Macro. Chem. **38**, 251–266 (2000).
32. S. Takagi, T. Shimada, T. Yui and H. Inoue, “High density adsorption of porphyrins onto clay layer without aggregation: characterization of smectite-cationic porphyrin complex,” Chem. Lett. **30**(2), 128–129 (2001).
33. Y. Ohtani, H. Nishinaka, S. Hoshino, T. Shimada and S. Takagi, “Anisotropic photochemical energy transfer in clay/porphyrin system prepared by size-matching effect and Langmuir–Blodgett technique,” J. Photochem. Photobiol. A **313**, 15–18 (2015).
34. H. C. van de Hulst, *Light Scattering by Small Particles*, (Dover Publishing, New York, 1981).
35. H. Monjushiro, A. Hirai and H. Watarai, “Size dependence of laser-photophoretic efficiency of polystyrene microparticles in water,” Langmuir **16**(22), 8539–8542 (2000).
36. T. Shoji, K. Itoh, J. Saitoh, N. Kitamura, T. Yoshii, K. Murakoshi, Y. Yamada, T. Yokoyama, H. Ishihara and Y. Tsuboi, “Plasmonic manipulation of DNA using a combination of optical and thermophoretic forces: separation of different-sized DNA from mixture solution,” Sci. Rep. **10**, 3349–3358 (2020).
37. C. E. Marshall, “The orientation of anisotropic particles in an electric field. Part I. General. Part II. Application to the determination of the double refraction of clays,” Trans. Faraday Soc. **26**, 173–189 (1930).
38. Q. R. Marvin, Chemical Research, *Optical Constants of Minerals and Other Materials from the Millimeter to the Ultraviolet* (Development & Engineering center, U.S. Army Armament Munitions Chemical Command. 1987), Chap. 4.
39. I. E. Borissevitchi, A. G. Bezerra-jr, A. S. L. Gomes, R. E. De Araujo, C. B. De Araujo, K. M. T. Oliveira and M. Trsic, “Z-scan studies and quantum chemical calculations of meso-tetrakis(p-sulfonatophenyl)porphyrin and meso-tetrakis(4-N-methyl-pyridiniumyl)porphyrin and their Fe(III) and Mn(III) complexes,” J. Porphyr. Phthalocya. **5**(1), 51–57 (2001).
40. Y. Harada and T. Asakura, “Radiation forces on a dielectric sphere in the Rayleigh scattering regime,” Opt. Commun. **124**(5), 529–541 (1996).
41. N. Malagnino, G. Pesce, A. Sasso and E. Arimondo, “Measurements of trapping efficiency and stiffness in optical tweezers,” Opt. Commun. **214**(1), 15–24 (2002).
42. M. Dienerowitz, M. Mazilu and K. Dholakia, “Optical manipulation of nanoparticles: a review,” J. Nanophoton **2**(1), 21875–21906 (2008).
43. G. Mie,“Beiträge zur Optik trüber Medien, speziell kolloidaler Metallösungen,” Ann. D. Physik **4**, 378–445 (1908).
44. R. Improta, C. Ferrante, R. Bozio and V. Barone, “The polarizability in solution of tetra-phenyl-porphyrin derivatives in their excited electronic states: a PCM/TD-DFT study,” Phys. Chem. Chem. Phys. **11**, 4664–4673 (2009).